RSC Advances




ROYAL SOCIETY OF CHEMISTRY

www.rsc.org/advances

Cite this: DOI: 10.1039/c0xx00000x

www.rsc.org/xxxxxx

ARTICLE TYPE

# Phase-induced porous composite microspheres sintered scaffold with protein-mineral interface for bone tissue engineering

**Janani Radhakrishnan‡, Gnana Santi Phani Deepika Gandham‡, Swaminathan Sethuraman and Anuradha Subramanian***

***Received (in XXX, XXX) Xth XXXXXXXXX 20XX, Accepted Xth XXXXXXXXX 20XX***
**DOI: 10.1039/b000000x**

Scaffold for orthopedic reconstruction should best mimic the microenvironment of bone to instil regenerative potential. In this study, three-dimensional porous microsphere sintered scaffold that closely resemble bone micro-architecture has been fabricated. Synthesized nanohydroxyapatite (~30-90 nm) using wet chemical precipitation and poly(hydroxybutyrate)/poly(ε-caprolactone) were blended to develop composite porous microspheres via emulsion induced phase separation. Brunauer–Emmett–Teller analysis reveals presence of cylindrical mesopores in microspheres with surface area (10.64$m^2$/g), which on solvent/non-solvent sintering to scaffold, resembles trabecular section of rat sternum. The scaffold demonstrates desirable compressive strength (1.16 ± 0.17 MPa) and compressive modulus (6.8 ± 1.3 MPa) with slow degradation and microstructrual stability for four weeks. Further, Incorporation of bovine serum albumin (BSA) in scaffold establishes protein-mineral interface and exhibits two-phase protein release mechanism (diffusion and polymer degradation). Pore interconnectivity and functional protein loading of scaffold have been evidenced by protein distribution analysis and secondary structural stability. The transverse section of MG63 cells cultured scaffolds with and without protein demonstrates cell infiltration and extension across the pores, while significantly higher proliferation is observed in protein scaffolds at day 7 ($p<0.05$). Hence, the biomimetic scaffold with protein-mineral interface could be an ideal substitute for bone regeneration as it establish cell-matrix interaction.

## Introduction

Patients suffering from bone disorders due to degeneration, medical or traumatic reasons are consistently increasing, which poses major clinical demand for functional bone tissue restoration [1]. Current clinical strategies such as use of autografts, allografts, xenografts and metallic implants suffer from various disadvantages like limited donor availability, donor site morbidity, disease transmission, long term inflammation, compliance mismatch, rejection, fibrous encapsulation, repetitive and prolonged surgery with significant cost issues [2-4]. These limitations stipulate the thorough investigations on smart material, which could imitate the physiology, composition and micro-architecture of native bone [5].

Bone is a natural composite of organic and inorganic substances, with ~30-70% of the later [6]. Nanohydroxyapatite ($Ca_{10}(PO_4)6(OH)_2$) (nHA), the major inorganic mineral present in bone provides strength and osteo-conductive properties [7]. Synthetic HA has been reported to be non-toxic, biocompatible and possesses excellent osteogenic properties with improved fracture toughness [8]. Further, it promotes scaffold-host tissue interactions and enhances new bone formation in a short duration [7, 9]. Conversely, brittleness and poor resorbability of the synthetic hydroxyapatite limits it potential applications in bone regeneration [10, 11]. Natural and synthetic polymers especially aliphatic polyesters are widely used in combination with HA for orthopaedic application, as they constitute the organic component of the bone matrix [12].

A hybrid Poly(hydroxybutyrate) (PHB)/HA functional scaffold has been reported to enhance the reparative osteogenesis [9]. Saos-2 cells adhered and proliferated on Poly(ε-caprolactone) (PCL)/HA scaffolds prepared by selective laser sintering processing confirming its potential for bone tissue engineering [13]. PHB is natural, tough polyester possessing good cellular recognition with the limitations of brittleness. PCL is a synthetic semi-crystalline aliphatic polyester showing good toughness and higher fracture energy with the lack of biological recognition [10]. Both these aliphatic esters possess other ideal characteristics such as excellent biocompatibility, very slow biodegradation providing structural stability to the scaffold support till the bone repairs and new tissue regenerates [5]. So far, none of the materials satisfy all the required criteria and hence, material properties have been improved by blending natural and synthetic polymers to achieve the desired characteristics and to compensate the limitations of parent polymers [14, 15]. Hence, in the present study we have prepared a blend of poly(hydroxybutyrate) and poly(ε-caprolactone) (PHB-PCL) with inorganic component (nHA) as

composite scaffolds for bone tissue engineering applications.

Administration of proteins like bovine serum albumin (BSA), recombinant proteins, osteogenic factors or drugs like antibiotics has been established as remedial strategy to influence biomineralization process, kindle endogenous regenerative potential or alleviate pain and prevent infection in challenging bone defects [16, 17, 18]. However, limitations of current delivery system such as rapid protein instability, requirement of high dose and concern of cancer incidence demand the ideal delivery system with improved efficiency [19]. Hence, scaffolds with well-defined architecture could be designed to release the trophic factors at the lesion to enhance the restoration of bone [20].

Success of bone tissue engineering depends on the development of three-dimensional scaffolds with protein-mineral interface that best mimics the native bone. Of the various bone scaffolds, microsphere based scaffold has been chosen as it mimics the micro-architecture of the native trabecular bone. Recently, development of porous microspheres for tissue engineering applications has gained much attention due to its greater surface area, lesser density, and outstanding absorption capability over conventional smooth microspheres [21]. Further, pores in between and on the surface of the microspheres of the sintered scaffolds would promote angio-neogenesis and cellular infiltration by facilitating the nutrient transfer throughout the scaffold [2, 21].

The major objective of the present study was to develop and characterize a 3-D composite porous microsphere sintered scaffold loaded with a model protein (BSA) for bone tissue regeneration. Solvent/non-solvent sintering was adopted as it can be performed in the presence of inorganic component (Hydroxyapatite), which cannot be temperature sintered and also for the encapsulation of temperature sensitive biological factors or proteins [22-26]. Proteins have major influence on the precipitation of calcium phosphates and BSA interaction with nHA has been reported to induce biomineralization [27]. The nHA synthesized by precipitation method has been combined with a blend of polyesters, PHB and PCL to fabricate composite porous microspheres using single emulsion technique. Solvent/non-solvent aid was used to sinter the composite porous microspheres with and without protein. The surface morphology, crystallinity, thermal stability, surface area of porous composite microspheres and the scaffolds were characterized. In addition, the degradation, compressive strength, protein distribution, in vitro protein release and stability of the 3D scaffolds was carried out to evaluate the potency of three-dimensional protein releasing composite porous microspheres sintered scaffold for bone tissue engineering.

## Materials and Methods

### Materials

PHB (MW: 550 kDa) and PCL (MW: 300 kDa) were purchased from Good fellow, UK and Lakeshore, USA respectively. Chloroform (GR), ammonia solution 25%, calcium nitrate tetrahydrate ($Ca(NO_3)_2.4H_2O$), diammonium hydrogen phosphate purified ($(NH_4)_2HPO_4$), were procured from Merck, India. Bovine serum albumin (BSA) (pH 7.0) was obtained from Himedia, India. Poly(vinyl alcohol) (PVA) (MW: 1,25,000) and absolute ethanol were purchased from SD Fine Chemicals Limited, India and used without any further purification. Human Osteoblast-like cells (MG63) were obtained from the cell repository of National Centre for Cell Science, India. Minimum essential medium (MEM) was procured from Sigma, USA. Fetal bovine serum albumin (FBS), phosphate buffered saline (PBS) and penicillin/streptomycin were obtained from Gibco, India

### Methods

#### Synthesis of nanohydroxyapatite (nHA)

Nanohydroxyapatite was synthesized using calcium nitrate tetrahydrate ($Ca(NO_3)_2.4H_2O$) and diammonium hydrogen phosphate ($(NH_4)_2HPO_4$) as calcium and phosphate precursors respectively, by wet chemical precipitation method [20]. Briefly, equimolar solutions of $(NH_4)_2HPO_4$ and $Ca(NO_3)_2.4H_2O$ were taken in volume ratio of 1.67 and pH was adjusted to ~11 using ammonium hydroxide solution. The white precipitate obtained was filtered, washed with distilled water to remove the byproducts, dried at 100-120°C for 4-5 hours and finally calcined at 500-600°C for 2½ hours. The nHA obtained was stored at room temperature until further usage.

#### Preparation of composite porous microspheres

Scheme 1A illustrates the formation of phase separation induced porous composite microspheres of nHA/PHB-PCL by single emulsion (o/w) technique using Ultra High Torque Stirring Motor (Wiggenhauser, USA). Briefly, continuous organic phase was prepared by dissolving PHB and PCL in chloroform at the weight ratio of 1:1, insoluble nHA was added to the organic phase in the ratio 1:2 and left for stirring overnight to obtain homogenous suspension of nHA in polymer phase (discontinuous phase). The mixture was added drop wise to 1% aqueous PVA solution (continuous phase) under constant stirring at 900 rpm for 3 hours. Perturbation of the discontinuous phase in the continuous aqueous phase causes polymeric chains redistribution leading to phase separation which in turn induces pore formation in microspheres. The microspheres were collected by centrifugation, washed with distilled water and lyophilized for 24 hours.

The lyophilized microspheres were weighed and the percentage of microspheres yielded was calculated using the following formula [28],

Yield % of microspheres = Weight of microspheres/ (Total Weight of polymer + nHA) × 100 (1)

#### Fabrication of porous composite microspheres scaffold with and without BSA by solvent/non-solvent sintering

Polymeric microspheres were sintered using solvent/non-solvent sintering technique where chloroform and ethanol were selected as solvent and non-solvent respectively [15, 29]. In brief, 30 mg of microspheres were wetted with solvent/non-solvent solution (1:3), vortexed for 10 seconds until uniform wetting, transferred to a cylindrical mould (5mmX 2.5mm) and allowed to dry in vacuum. Protein loaded scaffold was prepared similarly as mentioned above, with the addition of 0.6% BSA aqueous

solution to the solvent/non-solvent mixture.

**Physiochemical characterization**

*Scanning Electron Microscopy with Energy Dispersive X-ray Analysis*

Surface morphology of nHA, composite microspheres and sintered scaffolds was determined using a scanning electron microscope (SEM, JEOL JSM 6701F, Japan). The samples were sputter coated with gold and observed under SEM at an accelerating voltage of 3 kV [30]. Energy Dispersive X-ray Analysis (EDX) was used to reveal the presence and localization of prominent elements in the composites at an accelerating voltage of 15 kV.

*X-ray Diffraction Analysis*

Crystalline nature of the synthesized nHA and composite microspheres was studied using an X-ray diffractometer (XRD) (D8 Focus, Bruker, Germany) with Cu-Kα radiation of wavelength 1.5418 Å [31]. Diffraction pattern was examined for $2\theta$ values from 10° to 60° with a step size of 0.01°/minute. Crystallite size has been calculated by Scherrer's formulae as follows.

Thickness of crystallite, $\tau = k\lambda/\beta \cos\theta$ (2)

Where $k$ is the constant that depends on crystallite shape (0.89); $\lambda$ the x-ray wavelength (0.154); $\beta$ is the full width at half maximum intensity (FWHM) or integral breadth (54.88) and $\theta$ the Bragg angle.

*Fourier-Transform Infra-Red Spectroscopy*

The IR spectra of nHA, composite spheres and sintered scaffold was recorded using IR spectrophotometer (Spectrum 100, Perkin Elmer, USA). The samples were mixed with potassium bromide, pelletized using a hydraulic pelletizer and the analysis was performed in the range of 4000-450 $cm^{-1}$ with an average of 10 scans at a resolution of 1 $cm^{-1}$.

*Thermogravimetric analysis*

The thermal behavior of PHB, PCL, nHA, and nHA/PHB-PCL composites was evaluated by thermogravimetric analysis (TGA) [30]. The mass change as a function of temperature was recorded using thermogravimetric analyzer (TGA) (SDT Q600, TA Instruments, USA). Briefly, around 5 mg of sample was taken in alumina pan and heated from 23°C (room temperature) to 1000°C at a ramp of 10°C/minute under nitrogen atmosphere. The surface area, pore volume and pore size distribution of porous nHA/PHB-PCL composite microspheres were analyzed using $N_2$ adsorption–desorption isotherms (ASAP 2020, Micromeritics, USA) at 77K [32].

*Mechanical properties*

Compression test was performed using a uniaxial testing machine (INSTRON, USA) for cylindrical scaffolds (n=10) of diameter 5 mm and height 10 mm [33].The crosshead speed of 500 N load cell was set at 1 mm/minute until 60% of sample deformation. Compressive strength and compressive modulus was calculated as the maximum point of stress in the stress-strain graph and slope of the initial stress-strain curve respectively.

***In vitro* degradation studies**

*In vitro* degradation of the fabricated 3D composite sintered scaffolds (n=3) was assessed by immersing the scaffold in PBS (pH 7.4) for 5 weeks. The study was carried out at 37°C with continuous shaking using water bath shaker (Labline, India) and PBS was changed every two days. At predetermined time points, the scaffolds were collected, rinsed with PBS and lyophilized. The dried scaffolds were weighed and the morphological changes in the scaffolds were analyzed using SEM. The weight loss percentage was calculated by the following formula:

Weight Loss (%) = $[(W_i - W_d)/ W_i] \times 100$ (3)

Where, $W_i$ is initial weight of the sample, $W_d$ is dry weight of the sample

**Distribution of dansylated BSA**

Distribution of proteins on the microsphere scaffold and sintering sites were evaluated using confocal laser scanning microscopy (CLSM) (FV1000, Olympus, Japan). In brief, 0.2% dansyl chloride solution was prepared in acetone. The protein loaded porous microsphere sintered scaffold was immersed in 0.2% dansyl chloride solution for about 10 minutes to allow dansylation of BSA. The scaffold was imaged under confocal laser scanning microscope at an emission wavelength of 488 nm, followed by Z-sectioning and three dimensional reconstruction of the sample.

***In vitro* protein release kinetics & Mathematic modelling**

The BSA loaded scaffolds of 5 mm diameter and 4.5 mm height were immersed in 1 mL PBS at pH 7.4 and kept under continuous shaking using water bath shaker maintained at 37°C. At predetermined time intervals, the PBS was replaced with fresh PBS. The protein content was quantified based on Lowry's method and measured the absorbance at 690 nm using microplate reader (Infinite 200M, Tecan, USA) [34]. The mathematical modeling for the release of BSA was performed using DD solver software to evaluate the release kinetics.

**Circular Dichroism analysis**

The secondary structure stability of protein released from the scaffold was investigated and compared with protein in PBS and solvent/non-solvent interacted protein by circular dichroism (CD) analysis using spectropolarimeter (Jasco). About 5 mg/mL concentration of both native BSA and BSA released from scaffold were analyzed by spectropolarimetry at 25 °C. For assessing the effect of soft solvent sintering on the structural stability, BSA was dispersed in the solvent system used in the studied and separated out in PBS followed by spectropolarimetry analysis.

***In vitro* cell studies**

*Cell Seeding*

Human Osteoblast-like cells (MG63) were cultured in MEM supplemented with 10% FBS and 1% penicillin streptomycin as monolayer at 37°C in humidified atmosphere of 5% $CO_2$ and 95% air. The scaffolds were sterilized by exposing both sides to UV

light for 1 hour prior to cell seeding. For evaluating cell proliferation and infiltration, $5X10^4$ cells were seeded onto the scaffolds and tissue culture polystyrene (TCPS) used as control. The culture medium was changed every 24 h.

*Cell proliferation*

The osteoblast-like cells proliferation on scaffolds and TCPS by DNA assay as reported earlier [35]. Briefly, after 1, 3 and 7 days of culture, the culture media was removed from the wells, washed with PBS and 1 mL of distilled water was added. The well plates with distilled water were frozen at -70°C overnight followed by thawing at room temperature. The cells were lysed and DNA released by repeating the freeze-thaw cycles thrice. To another well plate, 50 µl of each sample and 50 µl of Tris–NaCl–EDTA (TNE) buffer was added followed by 100 µl of Hoechst stain working solution. The components were mixed well by tapping the plate and fluorescence was measured using Tecan at an excitation and emission wavelengths of 355 nm and 460 nm respectively. The cell number was assessed by calibration curve prepared for up to a density of $3.5 \times 10^6$ cells.

*Cell infiltration*

The cellular infiltration into the scaffolds was assessed using scanning electron microscopy. After 7 days of culture, media was removed and the scaffolds were washed with PBS prior to fixation using 4% glutaraldehyde at 4°C for 48 hours. The fixed samples were washed with PBS and dehydrated with graded alcohol concentration from 50 to 100%, followed by air–drying. The dried scaffolds were sliced transversely using a scalpel, sputter–coated with gold and observed using FE–SEM.

**Statistical Analysis**

Data are expressed as mean ± standard deviation obtained from at least three independent experiments. In order to determine the statistical significance between TCPS, sintered scaffold with and without protein, two-way analysis of variance followed by Tukey post-hoc test was performed for cell proliferation. SPSS 15.0 statistical software was used with $p < 0.05$ as criterion for statistical significance.

## Results and Discussion

Porous architecture and pore interconnectivity of the scaffold enhances the biological response of scaffold such as bone ingrowth and host-tissue integration but fail to meet the mechanical requirements of the native bone [36]. Although the use of hydroxyapatite ceramics for orthopaedic and dental applications dates back to 1980s, polymer/ceramic composite based scaffolds have been developed recently in order to improve the mechanical strength and scaffold-tissue integration [6]. However such composite microsphere based scaffolds lacks multi-scale porous architecture which plays vital role on vascularisation [7]. Hence designing a scaffold with excellent mechanical strength and desirable porous architecture could promote vascularization and cell infiltration in addition to the bio-integration [36]. The primary objective of the study involves the preparation of composite microspheres based scaffold with multi-scale porous structures in between as well as on the microspheres for bone regeneration.

Preparation of porous microspheres by methods such as particulate leaching, polymerization and seed swelling, suffers demerits such as presence of residuals such as reactants or porogens, protocol complexity and time consumption respectively [21], whereas the present study has established facile emulsion induced phase separation that overcomes the demerits and generate mesoporous structures in microspheres as illustrated in scheme 1A [37]. The quaternary phase diagram representing the thermodynamic stability of four components (PHB-PCL, nHA, organic solvent and aqueous phase) has been depicted in scheme 1B.

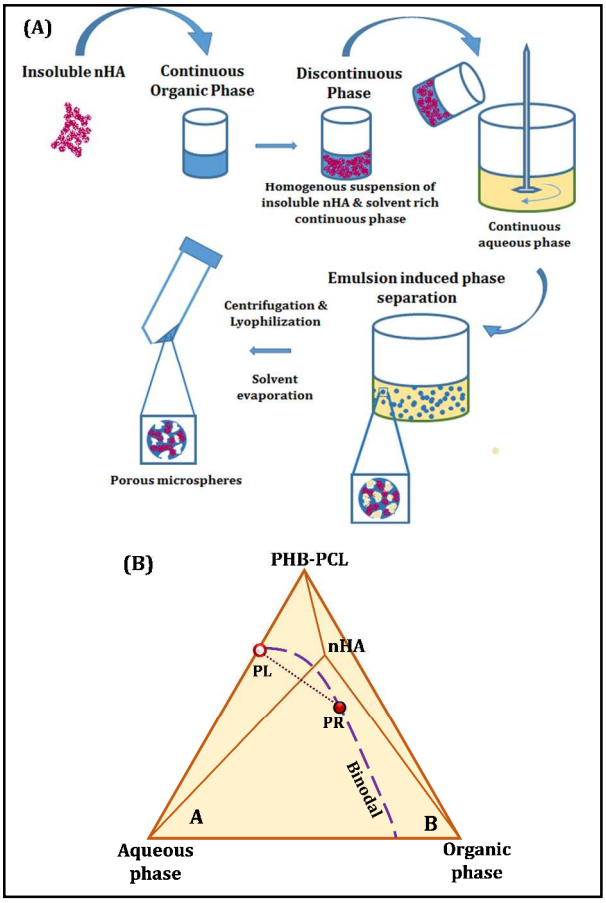


**Scheme 1** [A] The development of phase separation induced porous composite microspheres; [B] Quaternary phase diagram of the thermodynamic stability in the four components system

Nanohydroxyapatite stirred in continuous organic (polymeric) phase forms a homogenous suspension of insoluble nHA and solvent rich continuous polymer phase leading to discontinuity in phase (Region B - stable). On exposure to perturbation of the discontinuous phase in an insoluble continuous phase (Region A – unstable) at the binodal line, disturbance in the thermodynamic stability occurs when the two components (nHA and polymers) crosses the binodal. In order to lower the free energy of region A, liquid-liquid demixing occurs and redistribution of polymeric chains leads to the separation of two phases: polymer-rich (PR) and polymer-lean (PL) phases [38]. Further exchange of solvents causes solidification of the PR phase while the PL phase regions forms the porous structure on removal of solvents. The developed

porous composite microspheres thus formed were sintered to 3D scaffolds by dynamic solvent sintering, as thermal sintering mechanism fails to sinter thermally stable inorganic materials and denature heat labile proteins [29].

## Physico-chemical characterization

### Surface morphology and elemental composition

The surface morphologies, dimensions and elemental composition of the synthesized nHA, porous microspheres, composite porous microspheres and sintered composite microspheres scaffold were analyzed by SEM and EDX respectively. Figure 1A-B shows the as-synthesized nHA in the form of nano-sized irregular aggregates with size ranging between 30 and 90 nm. The EDAX spectrum of nHA (figure 1C) reveals the atomic weight percentage of calcium and phosphorus as 27.5% and 17% respectively at the ratio of ~1.6, which closely mimics the elemental composition of native bone (~1.67) [39].

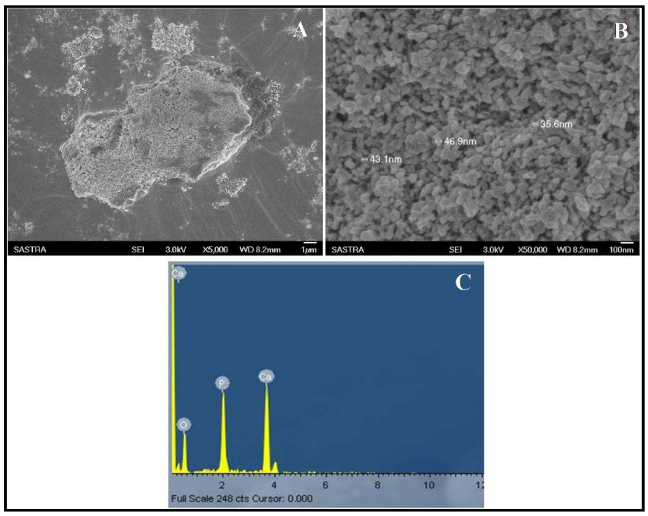


**Fig. 1** Scanning electron micrograph shows irregular aggregates of nHA at [A] low magnification and [B] at higher magnification. [C] EDAX spectra showing the presence of calcium and phosphorus, which are the major elements of nHA.

The scanning electron micrograph of the composite microspheres (nHA/PHB-PCL) prepared by single emulsion technique is shown in Figure 2A. Microspheres with porous morphology were obtained with a yield of 70-75% and the diameter ranged from 10 to 30 µm. Further EDAX spectrum (figure 2B) confirmed the presence of elements Ca and P of nHA at the ratio of ~1.6. The SE micrographs (figure 2C & D) exhibited the surface morphology of the solvent/non-solvent sintered composite porous microspheres scaffolds with and without BSA; the sintered sites were evident at higher magnification (figure 2E & F). The optical and SE micrographs of the trabecular section of rat sternum (figures 2G & H) exhibited multi-scale porous structures. The porosity of rat trabecular bone ranges between 50-90%, broadly similar to the human [40]. The morphology of the developed composite microspheres sintered scaffold exhibited multi-scale porosity that resembles the rat sternum trabecular or cancellous bone [41].

*FT-IR spectra*

Vibration spectra of nHA, PCL, PHB, composite microspheres, sintered scaffold with and without protein were characterized using IR to identify the functional groups (figure 3A & 3B) and characteristic bands were tabulated in Table 1. The characteristic bands at IR (KBr): $\nu$ = 565 $cm^{-1}$, 602 $cm^{-1}$,941 $cm^{-1}$, 1031 $cm^{-1}$, 1071 $cm^{-1}$ and 1090 $cm^{-1}$ of nHA corresponds to the various bending and stretching vibrations of phosphate groups, while the band at $\nu$ = 3446 $cm^{-1}$ represents hydroxyl group [42-44]. The bands at $\nu$ = 2945 $cm^{-1}$ ($CH_2$ asymmetric stretch), 2826 $cm^{-1}$ ($CH_2$ symmetric stretch), 1729 $cm^{-1}$ (O-C-O), 1459 $cm^{-1}$ ($CH_2$ bend) were observed in PCL [45], while additional bands at $\nu$ = 1292 $cm^{-1}$, 1279 $cm^{-1}$ and 1241 $cm^{-1}$ (C-O stretching), 1379 $cm^{-1}$ and 1368 $cm^{-1}$ ($CH_3$) were observed in PHB [46, 47]. The spectra of the composite microspheres and sintered scaffold showed characteristic bands of molecular vibrations confirming the presence of the polymers and nHA. Additionally, the characteristic bands clearly indicated that soft sintering has not affected the molecular vibrations of its constituents.

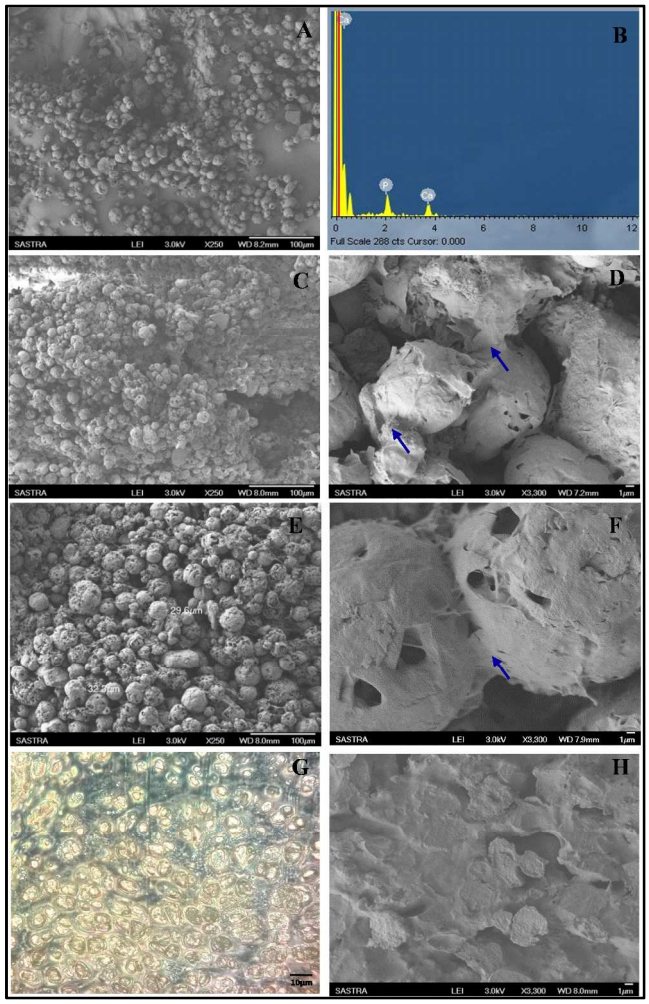


**Fig. 2** [A] Scanning electron micrograph of composite microspheres; [B] EDAX spectra showing the presence of calcium and phosphorus; the surface morphology of sintered scaffolds at [C] 250X and [D] 3300X (→ indicates the sintering sites). Micrograph of protein loaded scaffold at [E] 250X and [F] 3300X (→ indicates the sintering sites); [G] optical microscopic

image and [H] scanning electron micrograph of native bone showing the microarchitecture.

**Table 1** Bending and stretching vibrations of nHA, PCL and PHB in FT-IR spectra

| Functional groups | Mode of vibration | nHA | PHB | PCL | Composite microspheres | Sintered without protein | Sintered with protein |
|---|---|---|---|---|---|---|---|
| O-P-O | Bending | 565<br>602<br>(Strong) | | | 565<br>602 | 565<br>602 | 562<br>600<br>(Weak) |
| $PO_4^{3-}$ | Symmetric stretching | 941 | | | 960 | 960 | 962 |
| $PO_4^{3-}$ | Asymmetric stretching | 1031<br>1090 | | | 1040<br>1090 | 1040<br>1090 | 1045<br>1100<br>(Broad) |
| OH | Stretching | 3446 | | | | | |
| $CH_3$ | Bending | | 1379 | | 1380 | 1380 | 1380 |
| $CH_2$ | Bending | | 1459 | 1459 | 1459 | 1459 | 1459 |
| O-C-O | Stretching | | 1745 | 1729 | 1745 | 1745 | 1724 |
| $CH_2$ | Asymmetric | | 2945 | 2950 | 2990 | 2990 | 2990 |
| | Symmetric | | 2826 | 2825 | 2825 | 2825 | 2825 |

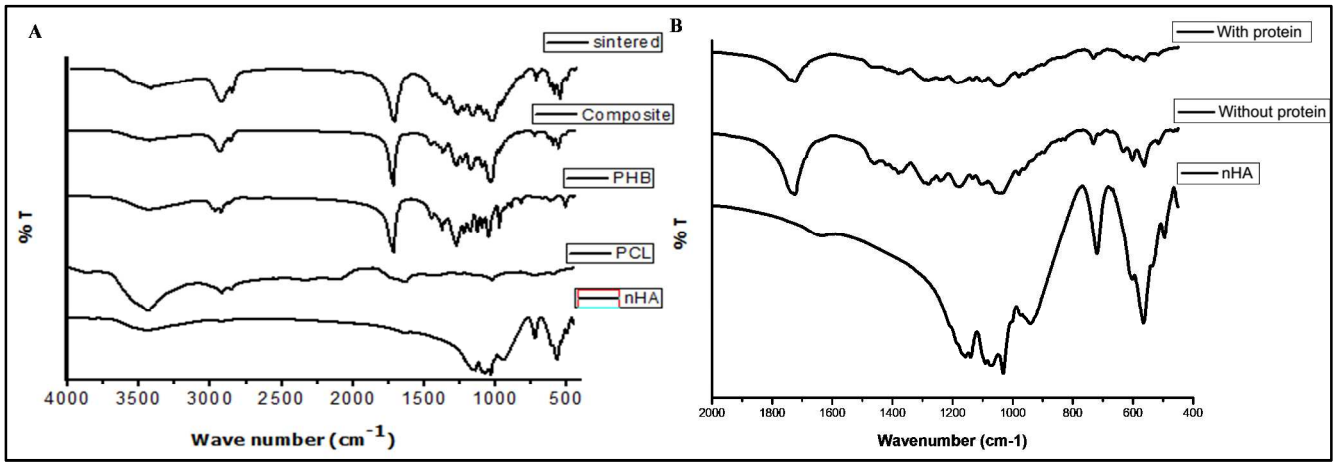


**Fig. 3** FTIR spectra of (A)the synthesized nHA, polymers PHB and PCL, nHA/PHB-PCL composite microspheres and solvent sintered composite microspheres, (B) nHA, sintered scaffold with and without protein

In order to analyze the interaction of BSA with nHA, the FTIR spectra of nHA, sintered scaffold with and without protein have been compared in figure 3B. On comparing the characteristic bending and stretching vibrations of $PO_4$ group at 560-616 $cm^{-1}$and 1030-1100 $cm^{-1}$ respectively (Table 1), noticeable reduction in the intensities and shift in the BSA loaded sintered scaffold was observed. This difference may be attributed to the presence of weaker dipole attraction between P-O in the $PO_4$ group of nHA, which may interact electrostatically with BSA [48]. Such protein-nHA interactions have the potential to induce biomineralization process to attain biochemical composition of bone tissue [18].

*X-ray Diffraction Analysis*

The crystallinity and crystal structure of nHA and composite microspheres were confirmed using X-ray diffractometer (Figure 4). The characteristic sharp peaks of nHA have been in accordance to the peaks of the native bone mineral reported previously [2, 42, 43]. The peaks at 25.8° and 32.1° in the composite confirmed the presence of nHA and the crystallinity was not altered during the formation of microspheres [49]. The broadening of the peaks in composite microspheres compared to nHA could be attributed to low crystallinity due to the presence of polymer [2, 50]. In natural bone, the nano-HA crystals and collagen make the overlap of the four peaks ranging from 32 to 35°. The XRD pattern of the composite has also been similar to natural bone mineral reported previously [2]. The prominent peaks in composite scaffold apart from the nHA peaks at 21.4° and 23.7° could be attributed to the polymers. The approximate crystallite size of nHA and composite microspheres were 7.828 nm and 37.39 nm respectively.

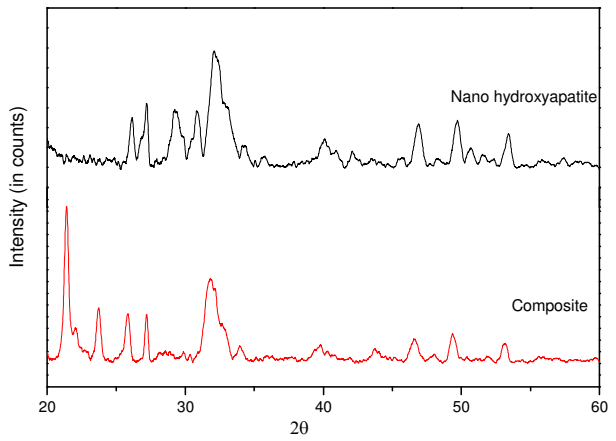


**Fig. 4** X-Ray diffraction pattern of nHA and nHA/PHB-PCL composite microspheres

*Thermogravimetric analysis*

Figure 5 shows the TGA/DTA thermographs of the polymers PHB, PCL, nHA and composite microspheres. The initial weight loss percentage of around 3.5% could be attributed to the removal of moisture content and the remaining 96.5% lasted without weight change till 1000°C for nHA. The lack of substantial weight loss percentage confirms the high thermal stability of inorganic hydroxyapatite, which restricts the sintering process at lower temperatures [51]. In contrast; steep weight loss at ~270-290°C and ~300-400°C in the thermographs of PHB and PCL respectively is due to the degradation of the polymers. In the thermograph of composite microspheres, the degradation of PHB and PCL was evident at ~280°C and ~380°C temperatures respectively. The 26.81% of content that remained up to 1000°C substantiated the presence of nHA in the composite microspheres. Thus, the thermo gravimetric analysis confirmed the blending of both organic polymers and inorganic nHA in the developed porous composite microspheres.

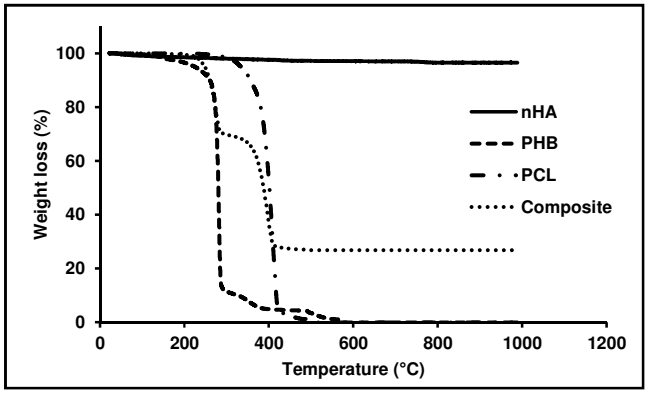


**Fig. 5** TGA-DTA thermographs of the synthesized nHA, polymers PHB, PCL, nHA/PHB-PCL composite microspheres

*BET analysis*

In order to investigate the characteristics of pores in the nHA/PHB-PCL composite microspheres, nitrogen adsorption–desorption isotherm was recorded (Figure 6).

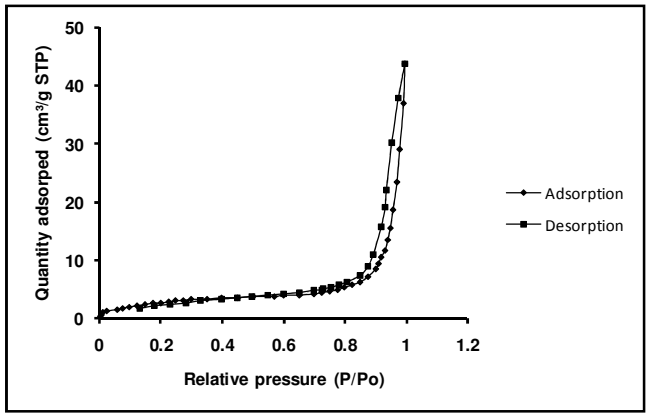


**Fig. 6** Nitrogen adsorption–desorption isotherm of mesopores in thenHA/PHB-PCL composite microspheres.

The isotherm pattern of the composite microspheres can be classified as type IV according to IUPAC nomenclature, which suggests the presence of mesoporous architecture [52]. The hysteresis pattern at above 0.6 P/P0 value confirmed the presence of cylindrical shaped pores [53]. The diameter of the pores in the microspheres ranged between 5-50 nm, with very few pores at 50-100nm and average diameter of the mesopores derived from BJH isotherm was found to be 34.34 nm. The pore volume of composite microspheres calculated from the BJH isotherm was found to be 0.0677$cm^3$/g, constituting to specific surface area of 10.64 $m^2$/g calculated using BET isotherm.

*Mechanical properties*

The mechanical property of bone (cortical and trabecular) is dependent on the anatomical location and the bone density value [54, 55]. The biomechanical properties of the porous composite sintered scaffold under dry condition were evaluated to analyze its load bearing capacity. The scaffold exhibited compressive strength of 1.16 ± 0.17 MPa and compressive modulus of 6.8 ± 1.3 MPa similar to previous reports which have proven promising candidates for bone tissue engineering [56, 57].

**_In vitro_ degradation of the composite sintered scaffolds**

The *in vitro* degradation behavior of composite sintered scaffold was evaluated for a period of 5 weeks. The percentage weight loss of the scaffold was recorded and their morphology was characterized using a scanning electron microscope (Figure 7) for 5 weeks. It was observed that the scaffolds lost about 2% of its initial weight after a week and gradually reached 13% at the end of 5 weeks (Figure 7A), showing slow degradation behavior of the composite sintered scaffolds. Morphology of the scaffolds observed from scanning electron micrograph showed that the scaffold retained its micro-structural stability up to 4 weeks essential for bone substituent candidate and disintegrated later after 5 weeks (Figure 7B-F). The porous nature of microspheres allows the faster diffusion of PBS leading to distortion of the microsphere structure. The probable mechanism of degradation of polyesters PCL and PHB employed in the composite could be by bulk hydrolysis of ester bonds [58, 59].

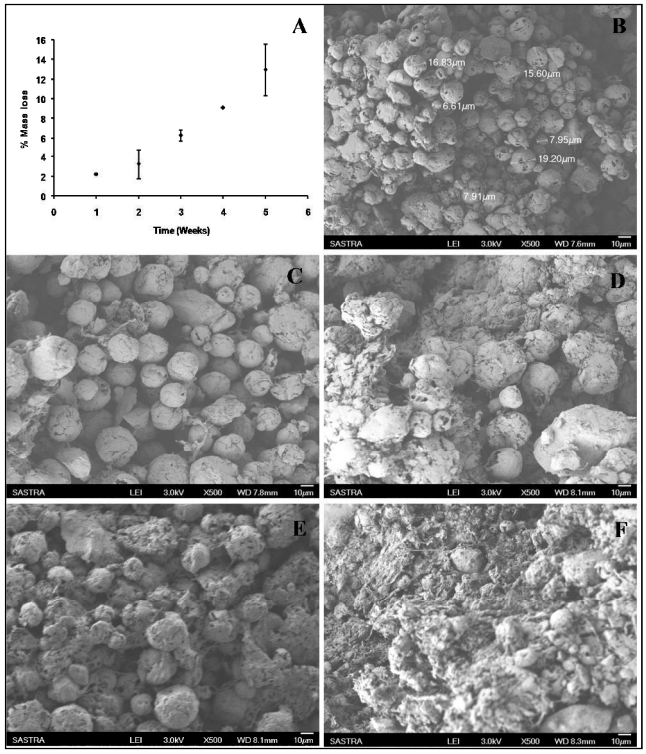


**Fig. 7** [A] *In vitro* weight loss of the scaffold as a percentage of the initial weight of the scaffold *in vitro* for a duration of 5 weeks, Scanning electron micrographs of nHA/PHB-PCL sintered degragded scaffoldsplaced in PBS for [B] 1 week; [C] 2 weeks; [D] 3 weeks; [E] 4 weeks and [F] 5 weeks. The change in morphology was noticeable from the third week

**Functional protein distribution in the sintered scaffold and *in vitro* release study**

*Confocal Laser Scanning Microscopy of dansylated protein*

The distribution of BSA that has been incorporated in the scaffold during sintering of microspheres was assessed quantitatively by dansylating BSA and subsequently imaging using confocal laser scanning microscopy. It was observed that though BSA has been integrated in the scaffold during sintering, it is prominently present throughout the scaffold (Figure 8A). The three dimensional construction of the CLSM Z-stacking shows the uniform distribution of BSA throughout the scaffold and the interconnected porous architecture of the scaffold, since it has allowed dansylation of protein in the deeper planes of the scaffold (Figure 8B).

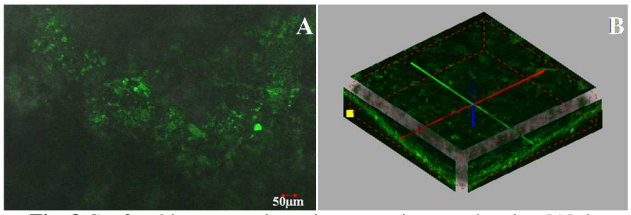


**Fig. 8** Confocal laser scanning microscopy images showing [A] the distribution of dansylated BSA on the scaffold; [B] three dimensional reconstruction of the scaffold shows the presence of BSA all over the scaffold

*In vitro BSA release kinetics and mathematical modelling*

A model protein BSA was loaded into the composite porous microsphere sintered scaffold during the solvent/non solvent sintering and their release profile was examined for a period of 5 weeks (Figure 9). It was observed that around 11.5% and 25.5% of protein was released in 1 day and 7 days respectively. The scaffold continued controlled release of protein leading to a cumulative release of 62% and 73% at the end of 21 and 35 days respectively. Thus, the release kinetics profile showed slow and sustained release up to 35 days, which can be attributed to the tight packing of spheres and slow degradation of the cylindrical microspheres scaffold (Figure 7).

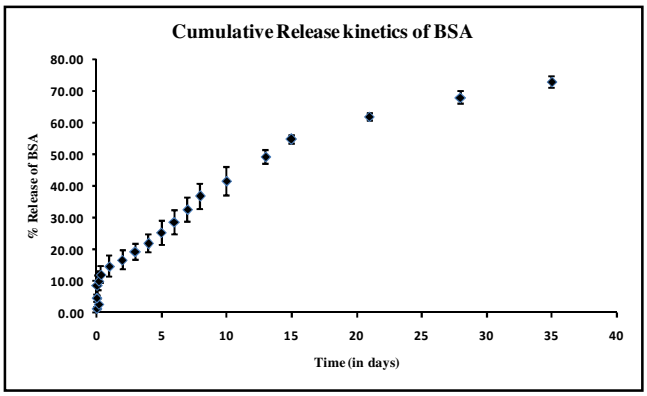


**Fig. 9** Cumulative release kinetics of BSA from sintered nHA/PHB-PCL microspheres scaffold

The mathematical modeling for protein release was evaluated to investigate the mechanism of release from the porous microspheres sintered scaffolds. The release data was analyzed using DDsolver 1.0 software for zero, first, Higuchi, Korsemeyer-Peppas, Hixson-Crowell, Baker-Lonsdale, Hopfenberg, Weibull, Gompertz and Makoid models. There was no linearity in the protein release profile recorded indicating that zero order kinetics was not been followed ($R^2$ 0.7075). The models that best fit the kinetics profile were Higuchi, Korsemeyer-peppas, Makoid, Baker-Lonsdale and Weibull models, their regression coefficient values have been listed in table 2. The $R^2$ value of 0.99 for Weibull model confirms the matrix type delivery system [60]. Higuchi model exhibits an $R^2$ value of 0.98 for describing that the protein diffusion from insoluble porous matrix through penetration of exterior liquid that dissolves the protein [61]. The kinetics data has also best fitted Korsemeyer-Peppas model with $R^2$ value of 0.98 and followed non-fickian anomalous transport thereby confirming the release of protein controlled by both diffusion and polymer relaxation [61, 62]. Further, higher $R^2$ value of 0.98 for Makoid model explaining the diffusion of proteins through the pores from slowly degrading polymers [58]. It was attributed that the high crystallinity, hydrophobicity and slow degradation of the polymers could also be contributing to the sustained release of the loaded moiety [58].

**Table 2** Release kinetics of BSA from composite porous microspheres sintered scaffold

| Kinetics model | K | R2 |
|---|---|---|
| Zero order | 0.115 | 0.707 |
| First order | 0.002 | 0.924 |
| **Higuchi** | **2.636** | **0.980** |
| **Korsemeyer-Peppas** | **2.807** | **0.980** |
| Hixson-Crowell | 0.001 | 0.884 |
| **Baker-Lonsdale** | **0.000** | **0.973** |
| Hopfenberg | 0.000 | 0.924 |
| **Weibull** | **152.889** | **0.988** |
| Gompertz | 2.807 | 0.934 |
| **Makoid** | **2.806** | **0.990** |

*Circular Dichroism Spectroscopy*

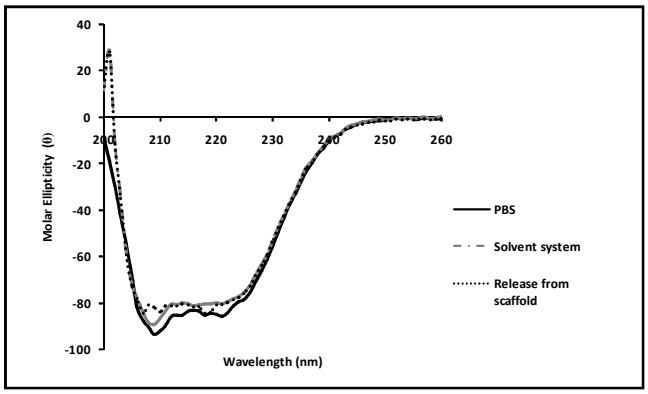


**Fig. 10** Circular dichroism spectra of BSA in PBS, in solvent system and BSA released from the nHA/PHB-PCL sintered microspheres scaffold

Figure 10 shows the CD spectra of BSA in PBS, BSA in the solvent system and BSA released from the scaffold to assess the effect of soft solvent sintering on the secondary structure of protein. The spectrum of the BSA in PBS (control) shows negative molar ellipticity at 200-245 nm similar to the spectra reported previously [63]. Further, the spectra recorded for BSA in the solvent and BSA released from scaffold does not show any significant alteration in the spectra profile. Thus, the analysis evidenced that the solvent sintering process did not alter the secondary structure of BSA, confirming protein stability in the sintered scaffold. This retention in the secondary structure of BSA released from the scaffold may be attributed to the electrostatic interaction between $PO_4^{3-}$ anion of nHA with $NH^{4+}$ cation of BSA, which is also confirmed by IR spectra.

**Osteoblast-like MG63 cells proliferation and infiltration**

The osteoblast-like cells proliferation and infiltration into the sintered scaffolds with and without protein were assessed by DNA quantification and SE microscopy respectively. Figure 11A represents the cell number in both the scaffolds and TCPS after 1, 3 and 7 days of culture. Although the cell number in the TCPS and both the scaffolds were comparable at days 1 and 3 ($p>0.05$), the sintered scaffold with protein promoted significantly higher cell proliferation at day 7 compared to TCPS ($*p<0.05$). Thus, the protein-mineral interface established in the scaffold has positively influenced the MG63 cell proliferation. The SE micrographs of transverse slice of scaffolds cultured with cells have been shown in figure 11B and 11C. The attachment and spreading of cells in the scaffolds were observed with extensions across the porous voids. The cell-cell and cell-matrix interactions were pronouncedly evidenced with MG-63 cells colonizing the entire scaffold. Hence, the developed scaffolds have promoted proliferation and facilitated infiltration of cells through the porous structure.

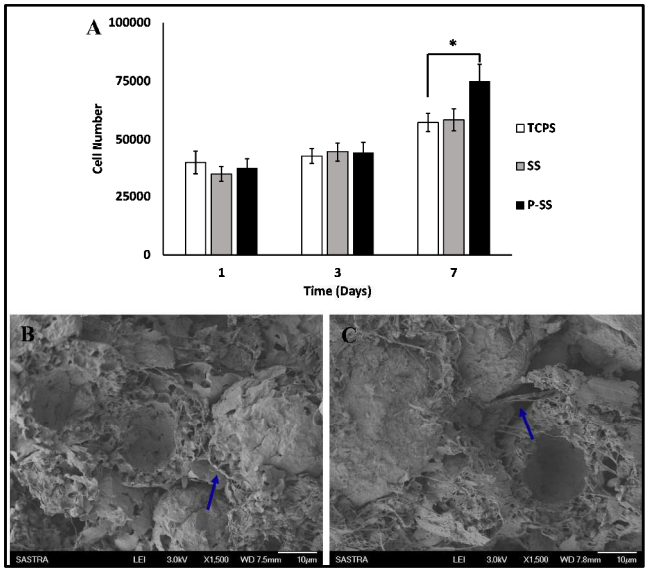


**Fig. 11**[A] Proliferation of MG63 cells in TCPS, sintered scaffold with and without protein determined by DNA assay at different time intervals (*p<0.05); SE micrographs of transverse slice of cells cultured sintered scaffolds [B] without protein (SS) and [C] with protein (P-SS) (→ indicates filopodial extension of cells)

## Conclusions

Phase separation induced porous nHA/PHB-PCL composite microspheres were prepared and solvent/non-solvent sintered to construct 3D cylindrical scaffolds for the bone tissue regeneration. In this scaffold, nHA synthesized by wet chemical precipitation constituted the inorganic component while the polymeric blend of PHB-PCL formed the organic component of the composite mesoporous microspheres. The 3D composite scaffold exactly mimics the native bone in terms of composition and multi-scale porous micro-architecture, thus possessing ideal scaffolding properties of bone with optimal mechanical strength. In addition, the protein loaded to the sintered scaffold interacts with nHA establishing protein-mineral interface and exhibited sustained release up to 35 days. Further, the mathematical modeling of the release suggested that the protein release was controlled by both diffusion through pores and polymer relaxation. CD analysis further explained that the solvent sintering does not alter the secondary structure of protein. Osteoblast-like cell studies have proved the potential of the scaffold to promote proliferation and infiltration. Hence, the developed scaffold could be a promising substrate for bone regeneration as it resembles the micro-architecture and inorganic content (nHA ~ 1.6) of native bone, accommodates osteoblast-like cells while also being able to deliver tropic factors.

## Acknowledgements

The authors wish to acknowledge Nano Mission (SR/NM/PG-

16/2007) and the FIST program (SR/FST/LSI-327/2007) of the Department of Science & Technology (DST), Government of India for their financial support. Prof. T. R. Rajagopalan R & D Cell of SASTRA University, Thanjavur, Tamil Nadu, India is acknowledged for financial support. First author is thankful to Innovation in Science Pursuit for Inspired Research (INSPIRE), Department of Science and Technology, India for Junior Research Fellowship (IF120692).

## Notes and references

*Centre for Nanotechnology & Advanced Biomaterials (CeNTAB), School of Chemical & Biotechnology, SASTRA University, Thanjavur – 613401, India. Fax: 91 4362 264120; Tel: 919443309910; E-mail: anuradha@bioengg.sastra.edu*

1 R. Zapatero, J. Barba, J. E. Canora, S. Losa, J. Plaza, R. San and J. Marco, *BMC Musculoskelet. Disord.* 2013, **14,** 15.
2 S. S. Liao, F. Z. Cui, W. Zhang and Q. L. Feng, *J. Biomed. Mater. Res. B Appl. Biomater.* 2004, **69,** 158.
3 I. O. Smith, X. H. Liu, L. A. Smith and P. X. Ma, *Wiley Interdiscip. Rev. Nanomed. Nanobiotechnol.* 2009, **1,** 226.
4 S. I. Roohani-Esfahani, S. Nouri-Khorasani, Z. Lu, R. Appleyard and H. Zreiqat, *Biomaterials* 2010, **31,** 5498.
5 D. Williams, *Materials today* 2004, **7,** 24.
6 A. N. Hayati, H. R. Rezaie and S. M. Hosseinalipour, *Materials Letters* 2011, **65,** 736.
7 J. R. Woodard, A. J. Hilldore, S. K. Lan, C. J. Park, A. W. Morgan, J. A. Eurell, S. G. Clark, M. B. Wheeler, R. D. Jamison and A. J. Wagoner Johnson, *Biomaterials,* 2007, **28,** 45.
8 A. Balamurugan, S. Kannan, V. Selvaraj and S. Rajeswari, *Trends Biomater. Artif. Organs.* 2004, **18,** 41.
9 E. I. Shishatskaya, I. A. Khlusov, T. G. Volova, *J. Biomater. Sci. Polym. Ed.* 2006, **17,** 481.
10 C. Hinüber, L. Häussler, R. Vogel, H. Brünig, G. Heinrich and C. Werner, *Express Polym. Lett.* 2011, **5,** 643.
11 B. Dhandayuthapani, Y. Yoshida, T. Maekawa and D. S. Kumar, *Int. J. Polym. Sci.* 2011, **2011,** Article ID 290602.
12 J. Liuyun, L. Yubao and X. Chengdong, *J. Biomed. Sci.* 2009, **16,** 65.
13 F. E. Wiria, K. F. Leong, C. K. Chua and Y. Liu, *Acta Biomater.* 2007, **3,** 1.
14 D. Liang, B. S. Hsiao and B. Chu, *Adv. Drug Deliv. Rev.* 2007, **59,** 1392.
15 J. L. Brown, L. S. Nair and C. T. Laurencin, *J. Biomed. Mater. Res. B Appl. Biomater.* 2008, **86,** 396.
16 M. Shi, J. D. Kretlow, A. Nguyen, S. Young, L. S. Baggett, M. E. Wong, F. K. Kasper and A. G. Mikos, *Biomaterials,* 2010, **31,** 4146.
17 J. Li, J. Hong, Q. Zheng, X. Guo, S. Lan, F. Cui, H. Pan, Z. Zou and C. Chen, *J. Orthop. Res.* 2011, **29,** 1745.
18 X. Feng-juan, Z. Ying and Y. Li-jiang, *Trans. Nonferrous Met. Soc. China.* 2009, **19,** 125.
19 S. Bose, M. Roy and A. Bandyopadhyay, *Trends Biotechnol.* 2012, **30,** 546.
20 E. Sachlos and J. T. Czernuszka, *Eur. Cell. Mater.* 2003, **5,** 29.
21 Y. Cai, Y. Chen, X. Hong, Z. Liu and W. Yuan, *Int. J. Nanomedicine.* 2013, **8,** 1111.
22 M. Singh, B. Sandhu, A. Scurto, C. Berkland and M. S. Detamore, *Acta Biomater.* 2010, **6,** 137.
23 M. Borden, S. F. El-Amin, M. Attawia and C. T. Laurencin, *Biomaterials* 2003, **24,** 597.
24 T. Jiang, W. I. Abdel-Fattah and C. T. Laurencin, *Biomaterials* 2006, **27,** 4894.
25 F. Sun, H. Zhou and J. Lee, *Acta Biomater.* 2011, **7,** 3813.
26 M. P. Ferraz, F. J. Monteiro and C. M. Manuel, *J Appl. Biomater. Biomech.* 2004, **2,** 74-80.
27 C. Yao, W. Xu, A. Ding and J. Zhu, *J. Chem. Sci.* 2009, **121,** 89.
28 T. Sudhamani, K. N. Reddy, V. R. R. Kumar, R. Revathi and V. Ganesan, *I.J.P.R.D.* 2010, **2,** 19.
29 S. P. Nukavarapu, S. G. Kumbar, J. L. Brown, N. R. Krogman, A. L. Weikel, M. D. Hindenlang, L. S. Nair, H. R. Allcock and C. T. Laurencin, *Biomacromolecules.* 2008, **9,** 1818.
30 A. Subramanian, U. M. Krishnan and S. Sethuraman, *Ann. Biomed. Eng.* 2012, **40,** 2098.
31 L. R. Jaidev, D. V. Bhavsar, U. Sharma, N. R. Jagannathan, U. M. Krishnan and S. Sethuraman, *J. Biomat. Sci.-Polym. E.* 2014, **25,** 1093.
32 R. K. Ravichandran, D. Sundaramurthi, S. Gandhi, S. Sethuraman and U. M. Krishnan, *Micropor. Mesopor. Mat.* 2014, **187,** 53.
33 S. Sethuraman, L. S. Nair, S. El-Amin, M. Nguyen, A. Singh, N. Krogman, Y. E. Greish, H. R. Allcock, P. W. Brown and C. T. Laurencin, *Acta Biomater.* 2010, **6,** 1931.
34 S. P. Slocombe, M. Ross, N. Thomas, S. McNeill and M. Stanley, *Bioresour. Technol.* 2013, **129,** 51.
35 J. Radhakrishnan, A. A. Kuppuswamy, S. Sethuraman and A. Subramanian, *J. Biomed. Nanotechnol.* 2015, **11,** 512.
36 W. Hao, Z. Wei, L. Xiong, L. Xiaohong, D. Ke, D. Rongquan, M. Yandong and W. Jie, *Acta Biomater.* 2013, **9,** 8413.
37 O. Oredein-McCoy, N. R. Krogman, A. L. Weikel, M. D. Hindenlang, H. R. Allcock and C. T. Laurencin, *Lab Chip.* 2009, **26,** 544.
38 D. L. Elbert, *Acta Biomater.* 2011, **7,** 31.
39 G. M. Cunniffe, F. J. O'Brien, S. Partap, T. J. Levingstone, K. T. Stanton and G. R. Dickson, *J. Biomed. Mater. Res. A.* 2010, **95,** 1142.
40 V. J. Cvetkovic, S. J. Najman, J. S. Rajkovic, A. Lj. Zabar, P. J. Vasiljevic, *Veterinarni Medicina.* 2013, **58,** 339.
41 S. Sethuraman, L. S. Nair, S. El-Amin, M. Nguyen, A. Singh, Y. E. Greish, H. R. Allcock, P.W. Brown and C. T. Laurencin, *J. Biomater. Sci. Polym. Ed.* 2011, **22,** 733.
42 S. Catros, F. Guillemot, E. Lebraud, C. Chanseau, S. Perez, R. Bareille, J. Amédée and J. C. Fricain, *IRBM.* 2010, **31,** 226.
43 A. A. Chaudhry, S. Haque, S. Kellici, P. Boldrin, I. Rehman, F. A. Khalid and J. A. Darr, *Chem. Commun.* 2006, **2006,** 2286.
44 A. Elkayar, Y. Elshazly and M. Assaad, *Bone and Tissue Regeneration Insights*. 2009, **2,** 31.
45 A. Elzubair, C. N. Elias, J. C. Suarez, H. P. Lopes and M. V. Vieira, *J. Dent.* 2006, **34,** 784.
46 F. C. Oliveira, M. L. Dias, L. R. Castilho and D. M. Freire, *Bioresour. Technol.* 2007, **98,** 633.
47 J. de Jong, B. Ankone, R. G. H. Lammertink and M. Wessling, *Lab Chip,* 2005, **5,** 1240.
48 S. K. Swain and D. Sarkar, *Appl. Surf. Sci.* 2013, **286,** 99.
49 Y. T. Ong, A. L. Ahmad, S. H. S. Zein, K. Sudesh and S. H. Tan, *Sep. Purif. Technol.* 2011, **76,** 419.
50 M. Meskinfam, M. S. Sadjadi and H. Jazdarreh, *World Academy of Science, Engineering and Technology.* 2012, **6,** 03.
51 J. Venkatesan, Z. Qian, B. M. Ryu, N. A. Kumar and S. Kim, *Carbohydr. Polym.* 2011, **83,** 569.
52 D. Malina, K. Biernat and A. Sobczak-Kupiec, *Acta Biochim. Pol.* 2013, **60,** 851.
53 P. Moura, C. B. Vidal, A. L. Barros, L. S. Costa, L. C. Vasconcellos, F. S. Dias and R. Nascimento, *J. Colloid Interface Sci.* 2011, **363,** 626.
54 M. Thommes, *Chem. Ing. Tech.* 2010, **82,** 1059.
55 R. Carter and W. C. Hayes, *J. Bone Joint Surg. Am.* 1977, **59,** 954.
56 B. Duan, M. Wang, W. Y. Zhou, W. L. Cheung, Z. Y. Li and W. W. Lu, *Acta Biomater.* 2010, **6,** 4495.
57 B. Mandal, A. Grinberg, E. S. Gil, B. Panilaitis and D. L. Kaplan, *PNAS.* 2012, **109,** 7699.
58 F. Barbato, M. I. L. Rotond, G. Maglio, R. Palumb and F. Quaglia, *Biomaterials.* 2001, **22,** 1371.

59 V. A. Livshits, A. P. Bonartsev, A. L. Iordanskii, E. A. Ivanov, T. A. Makhina, V. L. Myshkina and G. A. Bonartseva, *Polym Sci Ser B+*. 2009, **51,** 256.
60 S. A. Goldstein, *J Biomech.* 1987, **20,** 1055.
61 S. Dash, P. N. Murthy, L. Nath and P. Chowdhury, *Acta Pol. Pharm.* 2010, **67,** 217.
62 O. A. A. Ahmed, S. M. Badr-Eldin and T. A. Ahmed, *Int. J. Pharm. Pharm. Sci.* 2013, **5,** 179.
63 R. Sharma, R. B. Walker and K. Pathak, *Ind. J. Pharm.Edu. Res.* 2011, **45,** 25.

**Table of contents**

Phase induced porous composite microspheres were solvent/non-solvent sintered to construct 3D multi-scale porous biomimetic scaffolds with and without protein for bone tissue engineering.